NUMERICAL SOLUTION OF UNSTEADY ROTATIONAL FLOW PAST FIXED AND ROTARY WING CONFIGURATIONS

N. L. Sankar and B. E. Wake
Georgia Institute of Technology
Atlanta, GA

S. Y. Ruo and J. B. Malone
Lockheed Georgia Company
Marietta, GA

INTRODUCTION

This work describes the application of unsteady 3-D Euler and Navier-Stokes equations to transonic flow past rotor blades, and wing-alone configurations. The computer code used in this study was developed under the U. S. Army Research Office support at Georgia Tech. The transonic wing-alone calculations were supported by the Lockheed Georgia Company under the IRAD program.

OBJECTIVES

Methods based on the transonic small disturbance theory, and the full potential equation have matured to a point where they may be used by the industries for routine aeroelastic calculations. There is now the need to look at higher order techniques based on the Euler and the Navier-Stokes equations. The higher order solvers can serve two purposes. First, they provide a second estimate in situations where potential flow theory may fail (high transonic Mach numbers, strong shock waves), and provide benchmark runs for the validation of potential flow codes. Secondly, they allow the designer to study phenomena such as high angle of attack transonic maneuvers, supersonic fighter aerodynamics, and 3-D separated flow around highly loaded rotor blades.

1. To Describe a Solution Procedure for the Numerical Solution of the 3-D Compressible Viscous or Inviscid Flow

2. Apply this procedure to a number of fixed and rotary wing problems of interest

Figure 1

GOVERNING EQUATIONS

The equations governing three-dimensional unsteady compressible flow are the Navier-Stokes equations. If the viscous terms are neglected, the Euler equations result. The present solution techniques are designed to work efficiently with both the Navier-Stokes and the Euler equations. All calculations have been done on an algebraically generated body-fitted coordinate system (ξ,η,ζ), which is allowed to move with time and follow the motion of the solid. The flow properties of interest at a given time level are ρ : the density, u,v,w: the velocity of the fluid in an inertial coordinate system, and e: the total energy of the fluid per unit volume. The quantities U, V and W are the contravariant components of velocity along the ξ- , η- and ζ- directions respectively. Also, p is the pressure.

EULER EQUATIONS

$$q_\tau + E_\xi + F_\eta + G_\zeta = 0$$

$$q = J^{-1}\begin{vmatrix} \rho \\ \rho u \\ \rho v \\ \rho w \\ e \end{vmatrix} \qquad E = J^{-1}\begin{vmatrix} \rho U \\ \rho uU + \xi_x P \\ \rho vU + \xi_y P \\ \rho wU + \xi_z P \\ (e+P)U - \xi_t P \end{vmatrix}$$

$$F = J^{-1}\begin{vmatrix} \rho V \\ \rho uV + \eta_x P \\ \rho vV + \eta_y P \\ \rho wV + \eta_z P \\ (e+P)V - \eta_t P \end{vmatrix} \qquad G = J^{-1}\begin{vmatrix} \rho W \\ \rho uW + \zeta_x P \\ \rho vW + \zeta_y P \\ \rho wW + \zeta_z P \\ (e+P)W - \zeta_t P \end{vmatrix}$$

$$P = (\gamma-1)(e - \tfrac{1}{2}\rho(u^2+v^2+w^2))$$

Figure 2

The quantities ξ_x, ξ_y, ξ_z etc. are the metrics of the transformation computed numerically using standard second order accurate finite difference formulas. The quantity J is the Jacobian of transformation.

NAVIER-STOKES EQUATIONS

$$q_\tau + (E-E_v)_\xi + (F-F_v)_\eta + (G-G_v)_\zeta = 0$$

$$E_v = J^{-1} \begin{vmatrix} 0 \\ \xi_x\tau_{xx} + \xi_y\tau_{xy} + \xi_z\tau_{xz} \\ \xi_x\tau_{yx} + \xi_y\tau_{yy} + \xi_z\tau_{yz} \\ \xi_x\tau_{zx} + \xi_y\tau_{zy} + \xi_z\tau_{zz} \\ \xi_x\beta_x + \xi_y\beta_y + \xi_z\beta_z \end{vmatrix}$$

$$F_v = J^{-1} \begin{vmatrix} 0 \\ \eta_x\tau_{xx} + \eta_y\tau_{xy} + \eta_z\tau_{xz} \\ \eta_x\tau_{yx} + \eta_y\tau_{yy} + \eta_z\tau_{yz} \\ \eta_x\tau_{zx} + \eta_y\tau_{zy} + \eta_z\tau_{zz} \\ \eta_x\beta_x + \eta_y\beta_y + \eta_z\beta_z \end{vmatrix}$$

$$G_v = J^{-1} \begin{vmatrix} 0 \\ \zeta_x\tau_{xx} + \zeta_y\tau_{xy} + \zeta_z\tau_{xz} \\ \zeta_x\tau_{yx} + \zeta_y\tau_{yy} + \zeta_z\tau_{yz} \\ \zeta_x\tau_{zx} + \zeta_y\tau_{zy} + \zeta_z\tau_{zz} \\ \zeta_x\beta_x + \zeta_y\beta_y + \zeta_z\beta_z \end{vmatrix}$$

Figure 3

TURBULENCE MODEL

A two-layer eddy viscosity model developed by Baldwin and Lomax is used in this study (Ref. 1). For the mildly separated flows considered here this model has proved adequate. Here l_m is the mixing length in the inner layer, proportional to the distance from the wall, and the van Driest damping factor. In the outer layer, F_{max} is a measure of the velocity scales within the shear layer, while d_{max} is a measure of the length scale. At large distances from the shear layer the eddy viscosity is designed to approach zero through the use of the intermittency factor F_k.

- **Baldwin-Lomax two-layer algebraic model used for eddy viscosity.**
- **Inner Layer:**

$$\mu_T = \rho \ell_m^2 \omega \qquad \text{for} \quad d < d_c$$

$$\ell_m = (\kappa d)[1 - \exp(-d_+/A_+)]$$

$$d_+ = d(\rho \tau_w)^{1/2}/\mu$$

- **Outer Layer:**

$$\mu_T = .0168 \rho c_1 F_w F_k \qquad \text{for} \quad d > d_c$$

$$F_w = \min(d_{max} F_{max},\ c_2 d_{max} Q^2 / F_{max})$$

$$F_{max} = \max[\ell_m \omega / \kappa]$$

$$F_k = [1 + 5.5(c_3 d/d_{max})^6]^{-1}$$

$$Q = \max|V| - \min|V|$$

Figure 4

HYBRID ALGORITHM

In the present procedure, the time derivatives appearing in the governing equation are discretized using a two-point backward difference formula. The derivatives along the ξ- and ζ directions have been kept at the new time level (n+1) where the solution is sought. The spanwise (η-) derivatives have been explicitly evaluated using the latest available information at the inboard station during odd time steps and outboard station during the even time step. Thus, the computational stencil resembles a plane Gauss-Seidel algorithm, where the spanwise sweeps are performed in opposite directions on alternate iteration levels. It may be shown from a linear stability analysis that this technique leads to a stable algorithm.

Implicit Euler rule:

$$q^{n+1} = q^n + \Delta t \frac{\partial q}{\partial t}^{n+1}$$

Evaluate spanwise term explicitly:

$$q^{n+1} = q^n - \Delta t(\delta_\xi E^{n+1} + \delta_\eta F^{n,n+1} + \delta_\zeta G^{n+1})$$

where spanwise term alternates between:

$$\frac{F^{n+1}_{i,j+1,k} - F^{n}_{i,j-1,k}}{2\Delta\eta} \quad \text{and} \quad \frac{F^{n}_{i,j+1,k} - F^{n+1}_{i,j-1,k}}{2\Delta\eta}$$

Figure 5

TIME LINEARIZATION

The fact that some of the quantities are to be computed at the new time level (n+1) means that the resulting system of equations is algebraic, but highly nonlinear. To avoid an iterative solution of non-linear equations, the well known Beam-Warming linearization (Ref. 2) is applied to the flux terms along the ξ- and ζ directions. The result is a system of linear, block pentadiagonal equations in which the unknown is the 'delta' change in the flow properties between adjacent time levels.

Second-order expansion:

$$\mathbf{E}^{n+1} = \mathbf{E}^{n} + [\mathbf{A}^{n}](\mathbf{q}^{n+1} - \mathbf{q}^{n}) + O(\Delta t^{2})$$

$$\mathbf{G}^{n+1} = \mathbf{G}^{n} + [\mathbf{C}^{n}](\mathbf{q}^{n+1} - \mathbf{q}^{n}) + O(\Delta t^{2})$$

where A and C are the Jacobian matrices:

$$[\mathbf{A}] = \partial \mathbf{E}/\partial \mathbf{q} \quad \text{and} \quad [\mathbf{C}] = \partial \mathbf{G}/\partial \mathbf{q}$$

The following linear system results:

$$[\mathbf{I} + \Delta t(\delta_{\xi}\mathbf{A}^{n} + \delta_{\zeta}\mathbf{C}^{n})]\Delta \mathbf{q}^{n+1} = \mathbf{R}^{n,n+1}$$

$$\Delta \mathbf{q}^{n+1} = \mathbf{q}^{n+1} - \mathbf{q}^{n}$$

$$\mathbf{R}^{n,n+1} = -\Delta t(\delta_{\xi}(\mathbf{E}^{n} - \mathbf{E}_{v}^{n,n+1}) + \delta_{\eta}(\mathbf{F} - \mathbf{F}_{v})^{n,n+1} + \delta_{\zeta}(\mathbf{G}^{n} - \mathbf{G}_{v}^{n,n+1}))$$

Figure 6

APPROXIMATE FACTORIZATION

The direct inversion of the pentadiagonal block matrix equations is expensive. In literature, a number of techniques are available, based on the approximate factorization techniques such as L-U decomposition or ADI decomposition. The purpose of these techniques is to break up the coefficient matrix into smaller, easily inverted matrices. In this work an ADI factorization is used to arrive at a system of block tridiagonal equations, which may be inverted using the Thomas algorithm.

ADI Solution in the Airfoil Plane

Approximate factorization:

$$[I + \Delta t(\delta_\xi A + \delta_\zeta C)] = [I + \Delta t\delta_\xi A][I + \Delta t\delta_\zeta C] + O(\Delta t^2)$$

Gives two linear systems with block tridiagonal matrices:

$$[I + \Delta t\delta_\xi A]\Delta q^{*n+1} = R^{n,n+1}$$
$$[I + \Delta t\delta_\zeta C]\Delta q^{n+1} = \Delta q^{*n+1}$$

At every time step, the solver marches through the radial stations explicitly performing two matrix-inversion sweeps at each station.

Figure 7

ARTIFICIAL DISSIPATION TERMS

The use of pure central differences to advance hyperbolic, or weakly parabolic equations can lead to numerical instabilities. A variety of artificial dissipation forms have been suggested in literature to overcome this instability. In this work, a fourth order explicit dissipation form is used, and to allow large amounts of explicit dissipation to be used without instability, a second order implicit dissipation term is added to the left side.

- **Using central differencing alone leads to odd-even decoupling.**
- **Nonlinearities of the equations produces high-frequency errors which grow.**
- **Second-order implicit dissipation and fourth-order explicit dissipation used.**
- **Fourth-order implicit dissipation stabilizes the scheme even more, but results in penta-diagonal systems.**
- **It can be shown that the dissipation results in an upwinded scheme.**

Figure 8

FINAL FORM OF THE DIFFERENCE EQUATIONS

The final form of the discretized equations, used in the computer code are shown below.

$$[I + \Delta t \delta_\xi \mathbf{A} - \Delta t \epsilon_i J^{-1} \nabla_\xi \Delta_\xi J] \Delta \mathbf{q}^{*n+1} = \mathbf{R}^{n,n+1} - \mathbf{D}_e{}^{n,n+1}$$

$$[I + \Delta t \delta_\zeta \mathbf{C} - \Delta t (\epsilon_i + \epsilon_\mu) J^{-1} \nabla_\zeta \Delta_\zeta J] \Delta \mathbf{q}^{n+1} = \Delta \mathbf{q}^{*n+1}$$

where, the explicit dissipation is:

$$\mathbf{D}_e{}^{n,n+1} = \Delta t \epsilon_E J^{-1} [(\nabla_\xi \Delta_\xi)^2 + (\nabla_\eta \Delta_\eta)^2 + (\nabla_\zeta \Delta_\zeta)^2] J \mathbf{q}^n$$

and the variable implicit coefficient is:

$$\epsilon_\mu = (\mu + \mu_T)(\zeta_x^2 + \zeta_y^2 + \zeta_z^2)$$

As an example,

$$(\nabla_\xi \Delta_\xi)^2 J \mathbf{q}^n = (\hat{\mathbf{q}}_{i+2} - 4\hat{\mathbf{q}}_{i+1} + 6\hat{\mathbf{q}}_i - 4\hat{\mathbf{q}}_{i-1} + \hat{\mathbf{q}}_{i-2})^n$$

$$(\nabla_\xi \Delta_\xi) J \mathbf{q}^n = (\hat{\mathbf{q}}_{i+1} - 2\hat{\mathbf{q}}_i + \hat{\mathbf{q}}_{i-1})^n$$

Figure 9

TREATMENT OF ROTOR WAKE

In helicopter applications, the treatment of the shed tip vortices requires special considerations. The finite difference grid is usually not large enough or fine enough to capture the many revolutions of the tip vortices shed by several blades. In this work, only the portion of the shed vorticity immediately downstream of the rotor blade is captured by the finite difference scheme. The rest of the vorticity, and the wake behind the other blades is kept track of using a Lagrangean approach. This approach was first proposed by Tung and Caradonna (Ref. 3).

- **Downwash due to tip vortex significantly affects the lift of the blade**
- **Resolving the tip vortex by finite difference techniques is not possible with current computer resources**
- **Effects of tip vortices lying outside of the computational domain must be included**

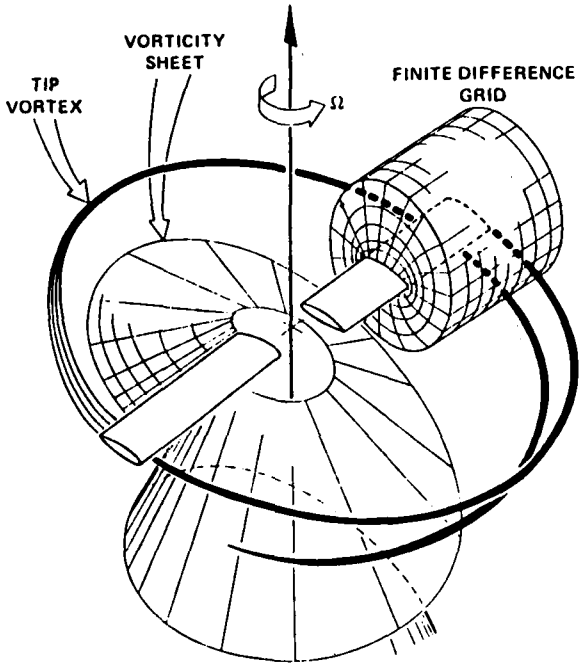

- **Use CAMRAD or some other wake code to obtain effective partial angle of attack distribution**

Figure 10

LIFTING VISCOUS FLOW PAST A HOVERING ROTOR

As a first application of the solution technique described, the subsonic lifting flow past a two bladed rotor system in hover is considered. The blades were made of NACA 0012 airfoils and had a rectangular planform. The collective pitch was 8 degrees, and the tip Mach number was 0.44. There is an extensive set of experimental data available for this configuration (Ref. 4). Here, the computed pressure distrbution at a number of radial stations is plotted and compared with experimental data. Good agreement is observed at all locations.

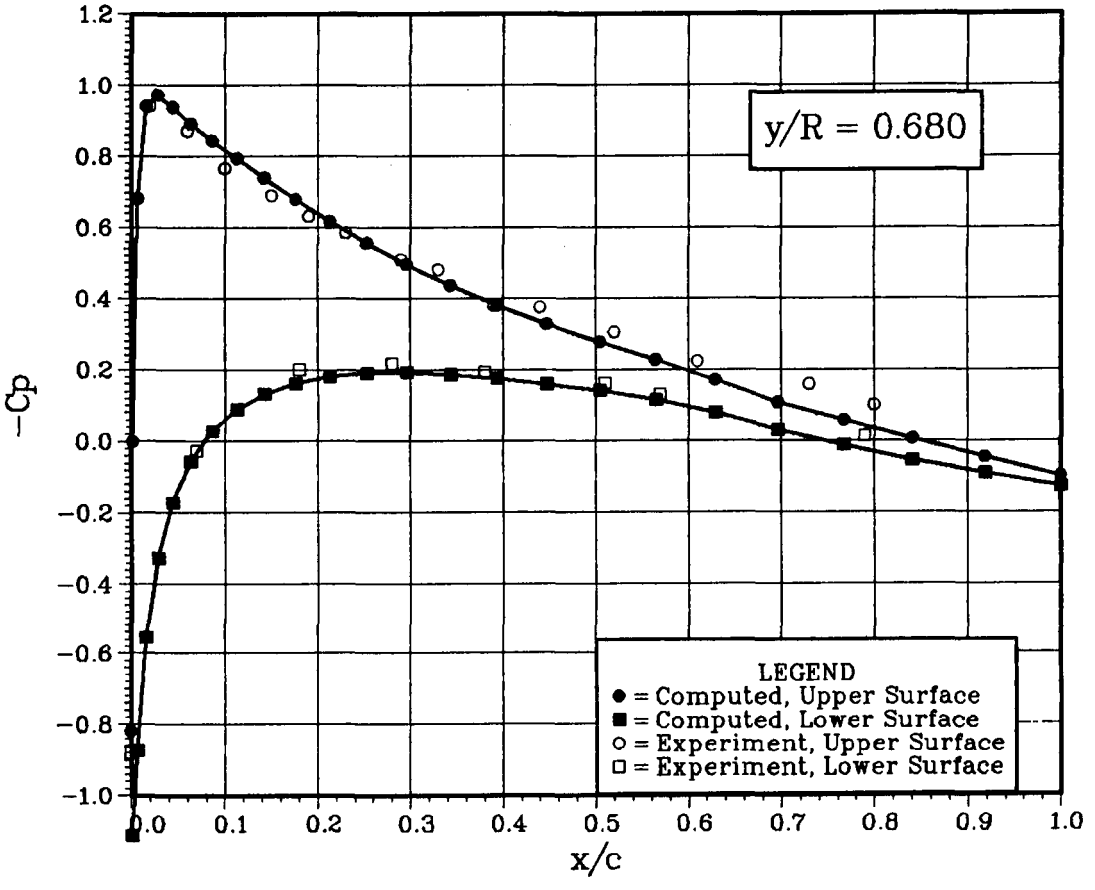

Figure 11

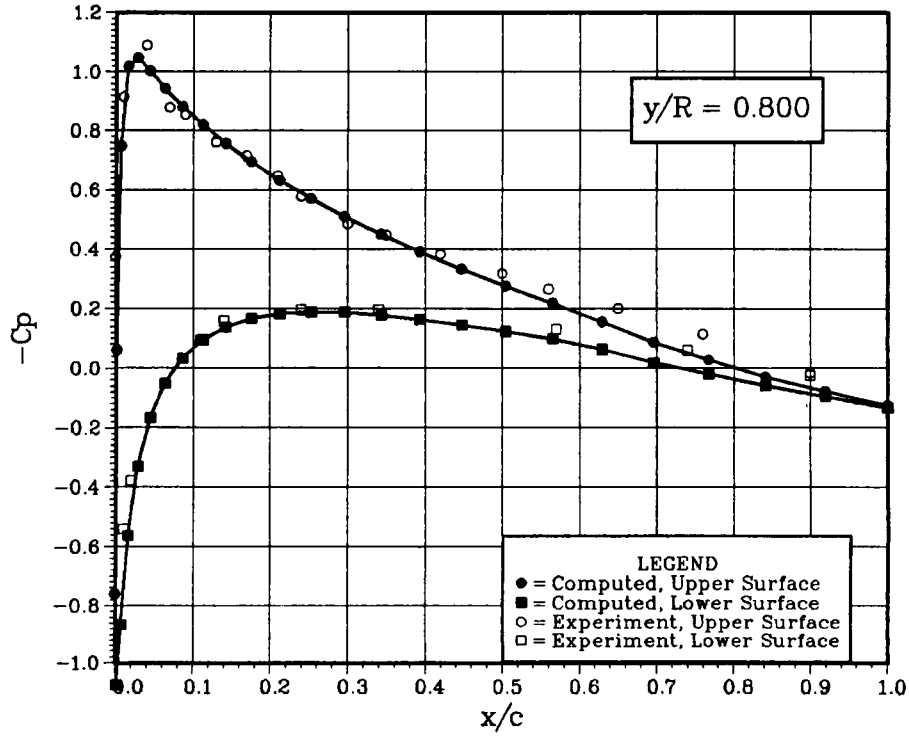

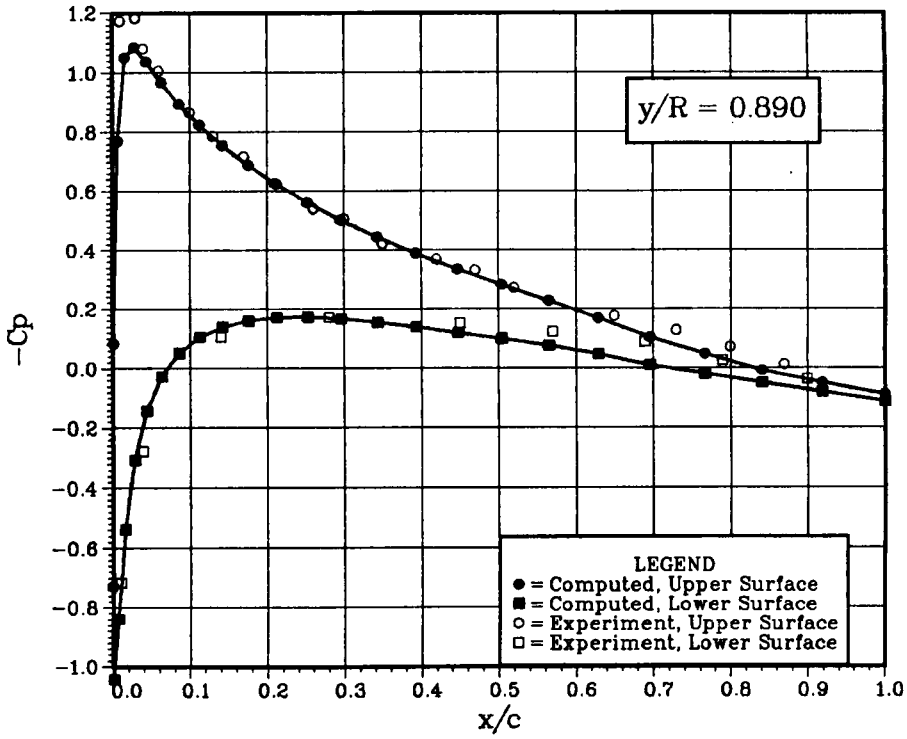

Figure 11 Concluded.

SPANWISE LOADING ON A HOVERING ROTOR

The integrated lift distributions are plotted along the rotor radius below. It is seen that good agreement with experiments is found.

These calculations were done on a 79 x 23 x 45 grid with 50 points at each radial location on the rotor, 11 radial locations on the rotor and 45 points in the normal direction. They required 3.9 seconds per time step on the CRAY XMP.

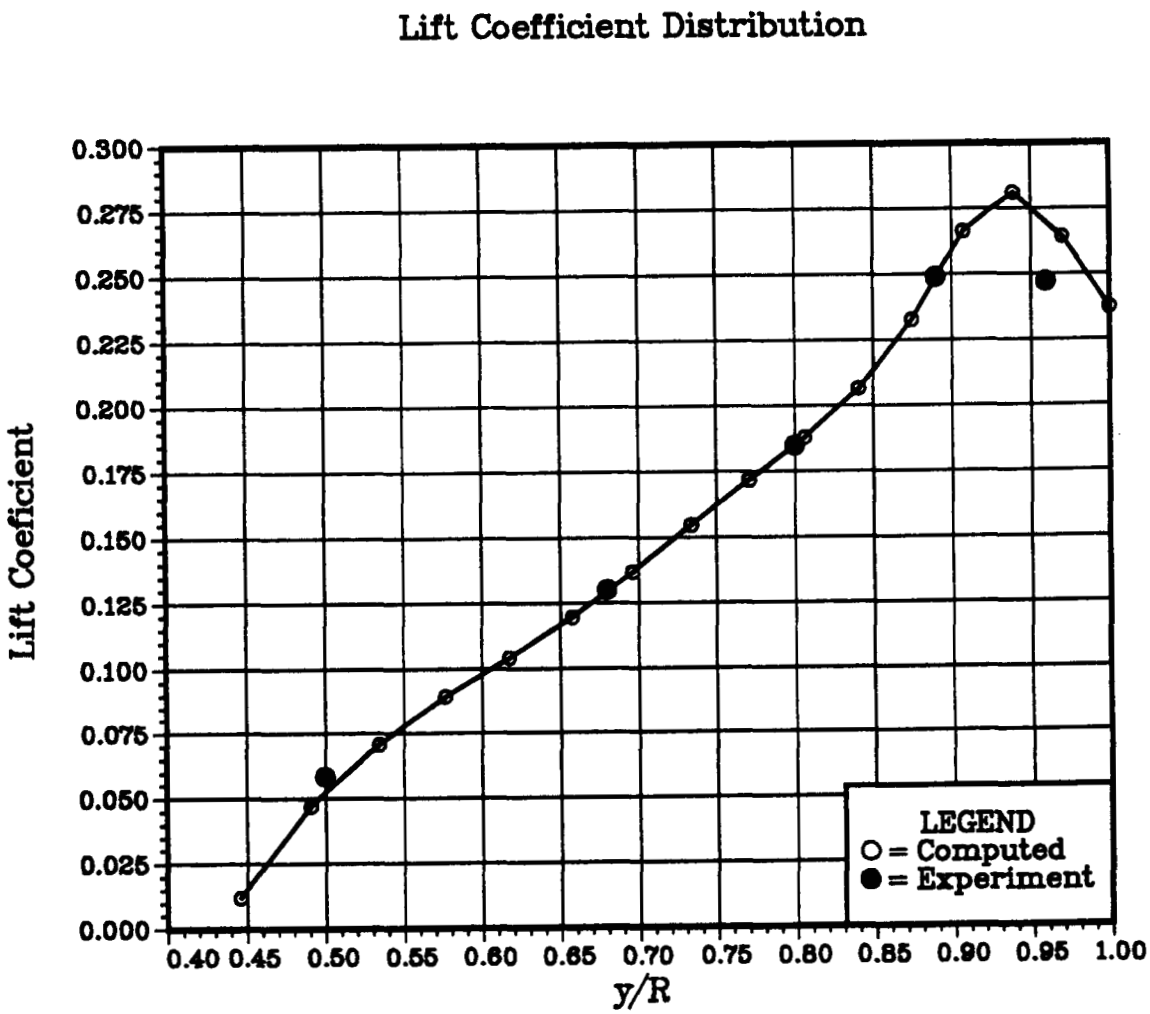

Figure 12

NON-LIFTING TRANSONIC FLOW OVER AN ADVANCING ROTOR

As a second example, the transonic viscous flow past a rotor blade tested at ONERA is considered. The tip Mach number in this case was 0.6, while the advance ratio (forward speed/tip speed) was 0.45. In the next several pages, comparisons between experiments and the Navier-Stokes solutions are given at the 84% span station. For the sake of completeness some Euler solutions are also shown. It is seen that both the Euler and the Navier-Stokes solutions give acceptable agreement with experiments. It is also seen that the Navier-Stokes results predict the shock locations and strength more accurately. These calculations were done on a 121 × 19 × 45 grid and required 4.6 sec per iteration on a CRAY XMP. Several thousand time steps were needed to advance the solution from zero degree azimuth to 360 degree azimuth in time, (through a full revolution).

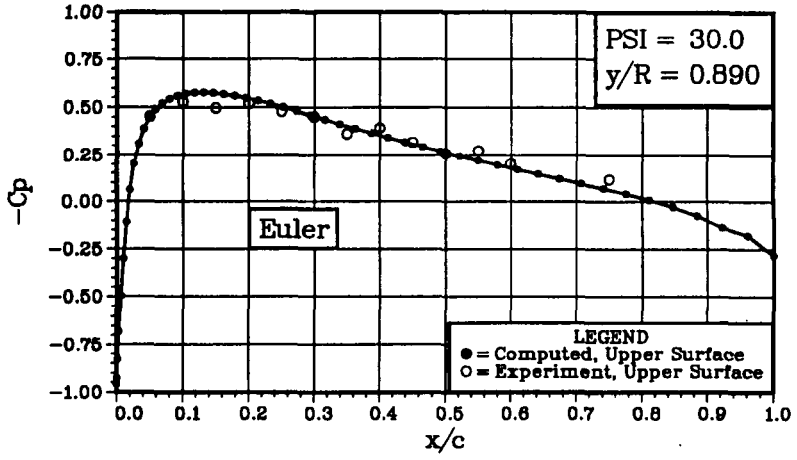

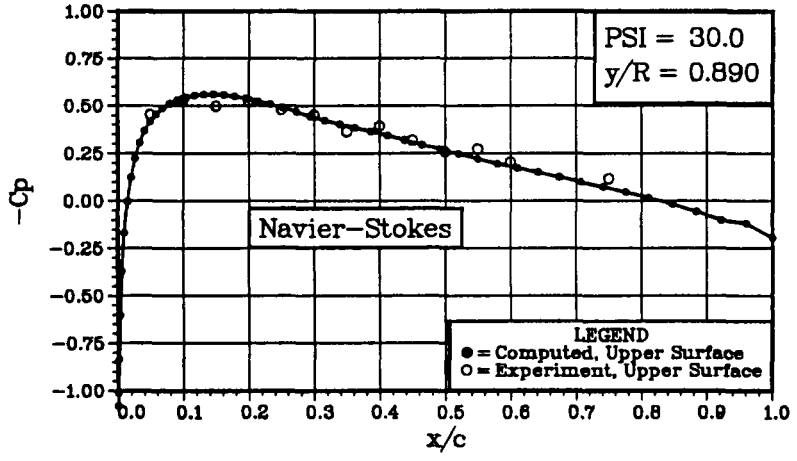

Figure 13

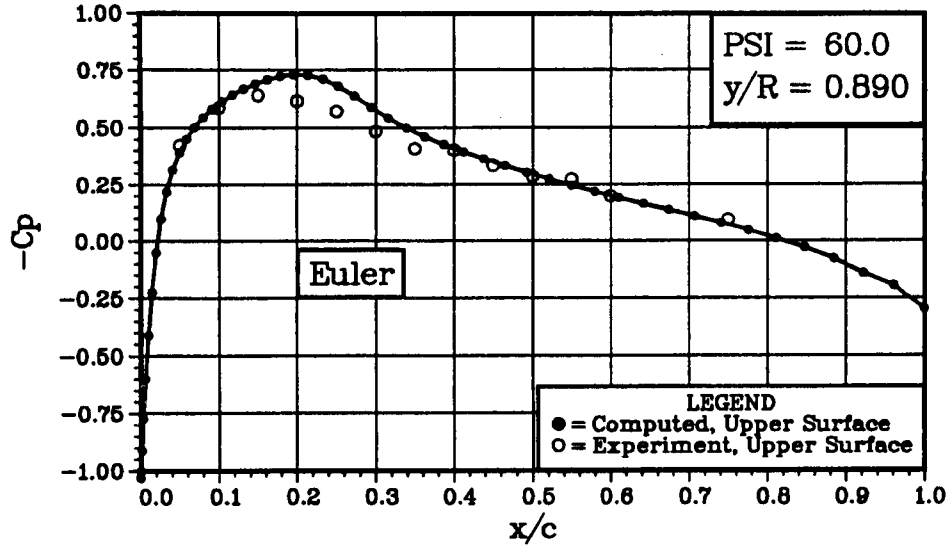

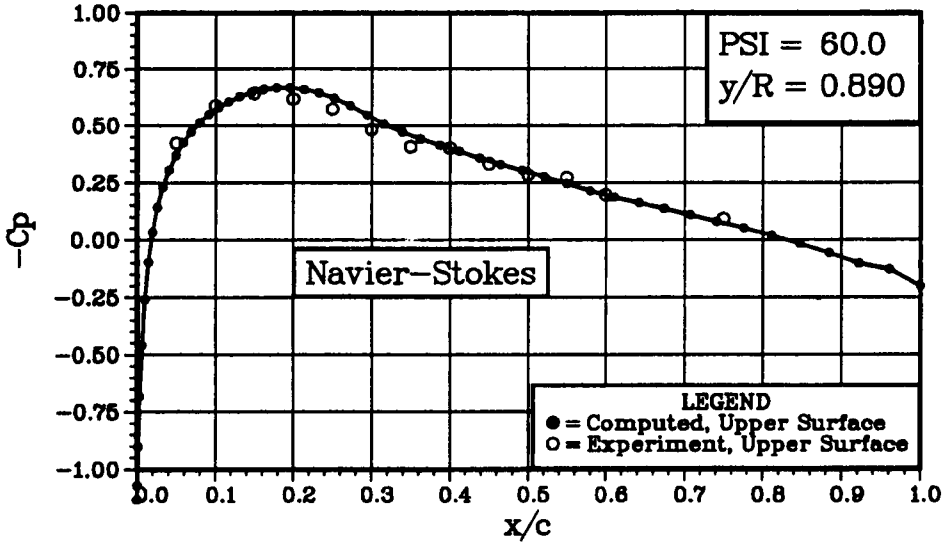

Figure 13 Continued.

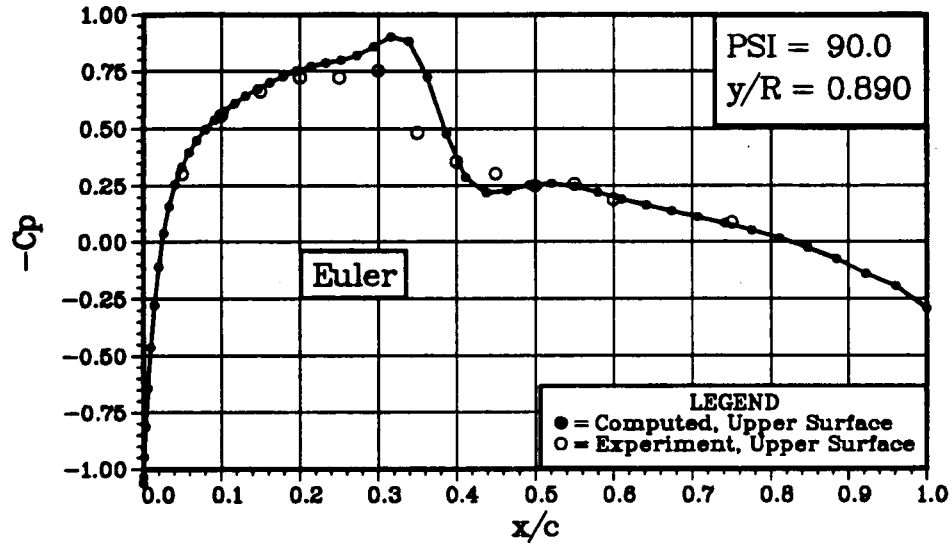

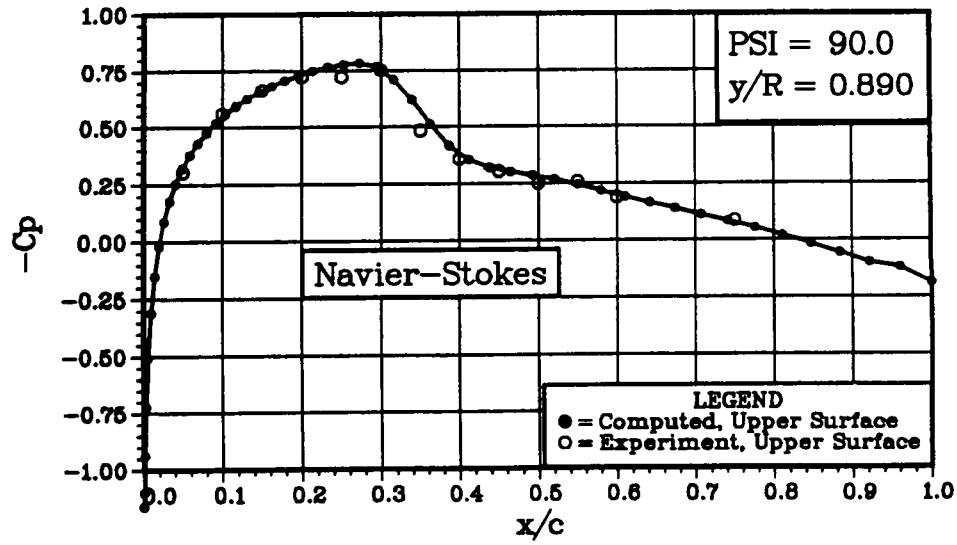

Figure 13 Continued.

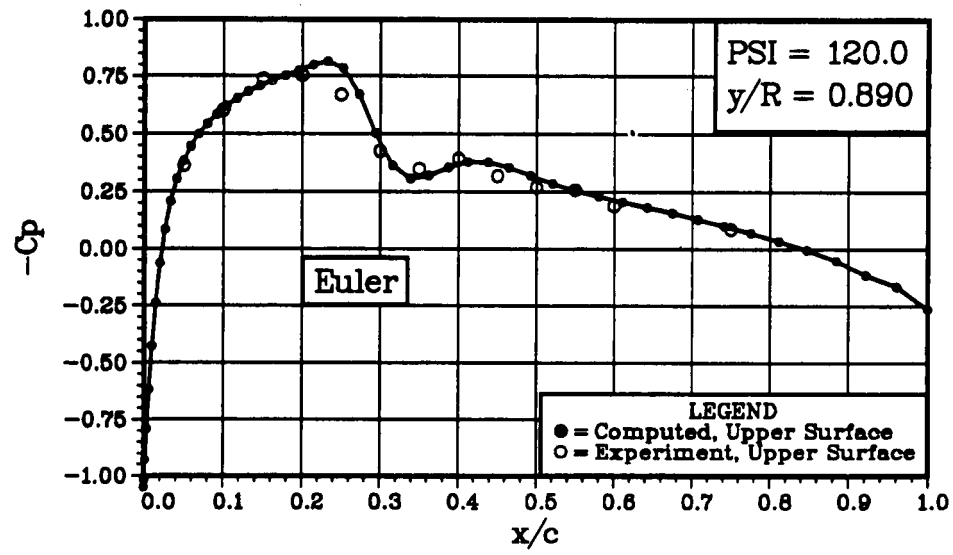

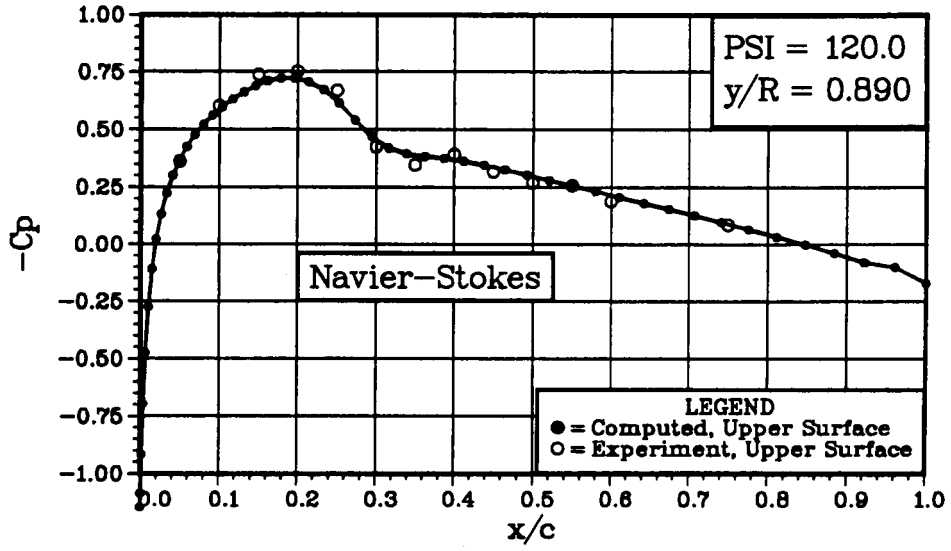

Figure 13 Continued.

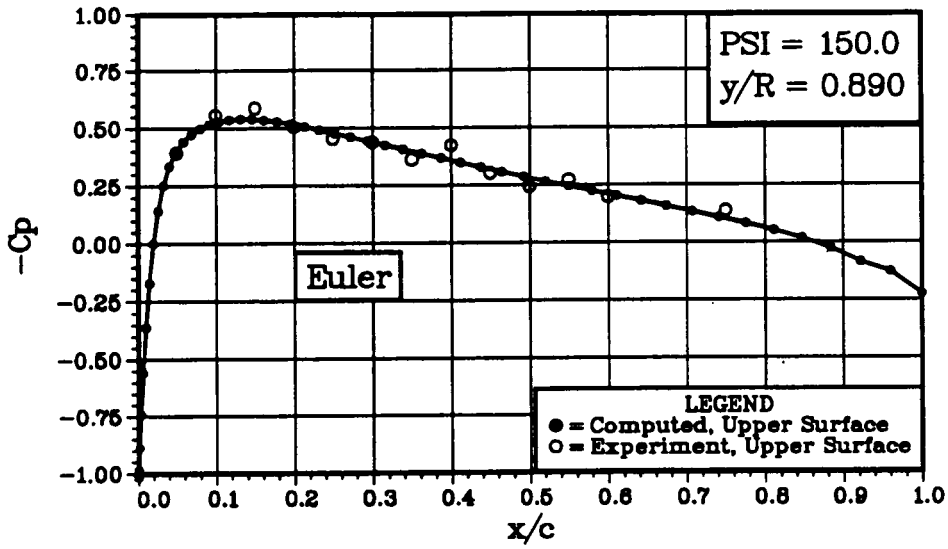

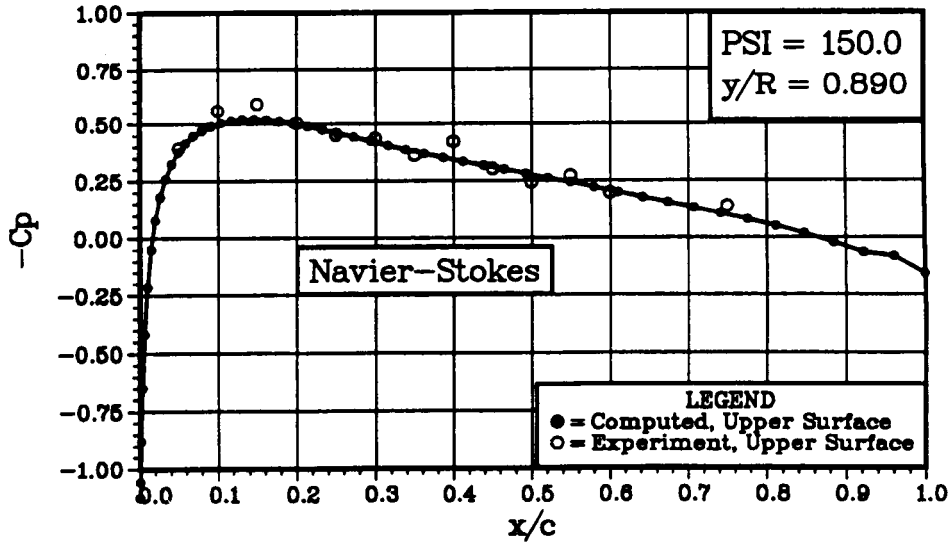

Figure 13 Concluded.

LIFTING TRANSONIC FLOW PAST A RECTANGULAR WING

As a final application of the present approach, the unsteady transonic flow past a rectangular supercritical wing tested at NASA Langley Research Center is presented. The freestream Mach number was 0.7 and the mean angle of attack was 1.98 degrees. The wing was constrained to oscillate in pitch at a frequency of 10 Hz. In the following figures, the in-phase and the out-of-phase components of the surface pressure distribution are plotted at several locations. Overall, a reasonably good agreement is observed.

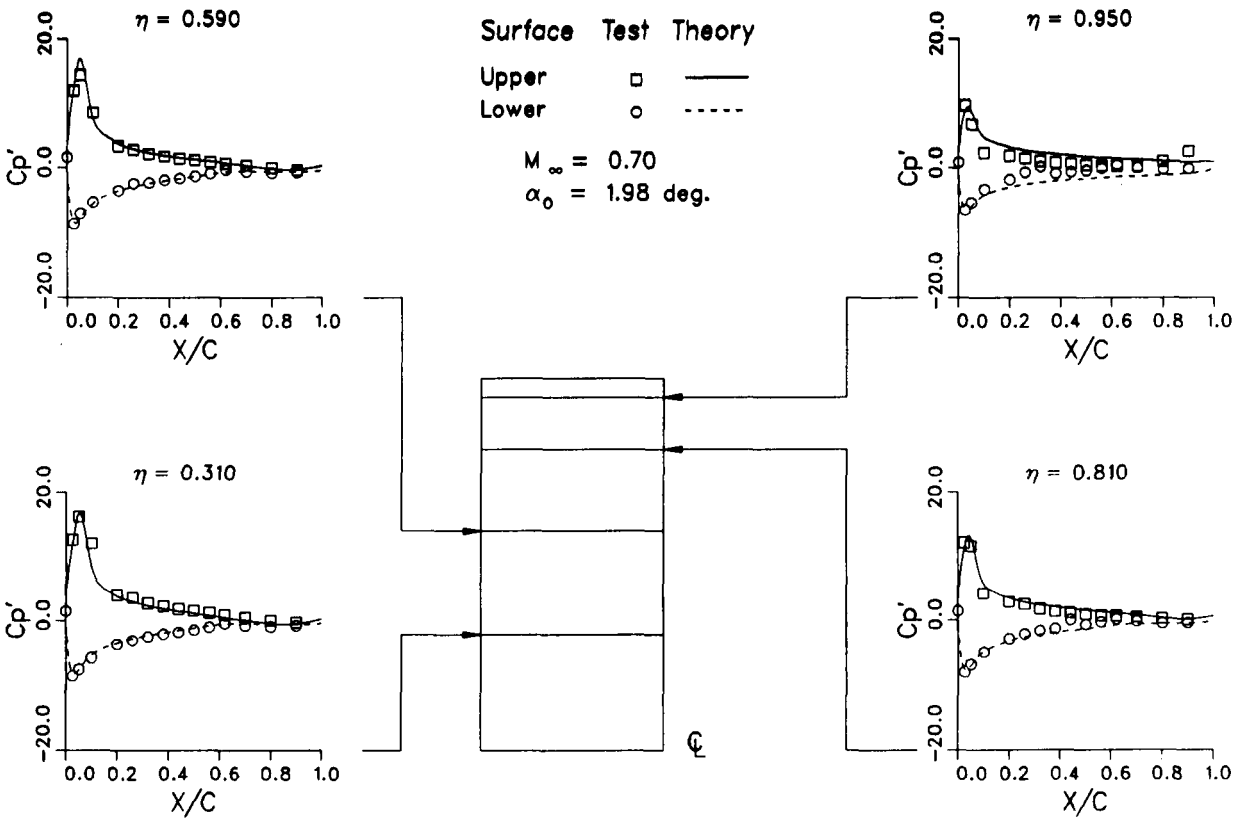

FIGURE 14. R376E21 INVISCID REAL AMPL=1.044 2000 S/C 5000 S , M_∞ = 0.70, α_0 = 2.0 deg.

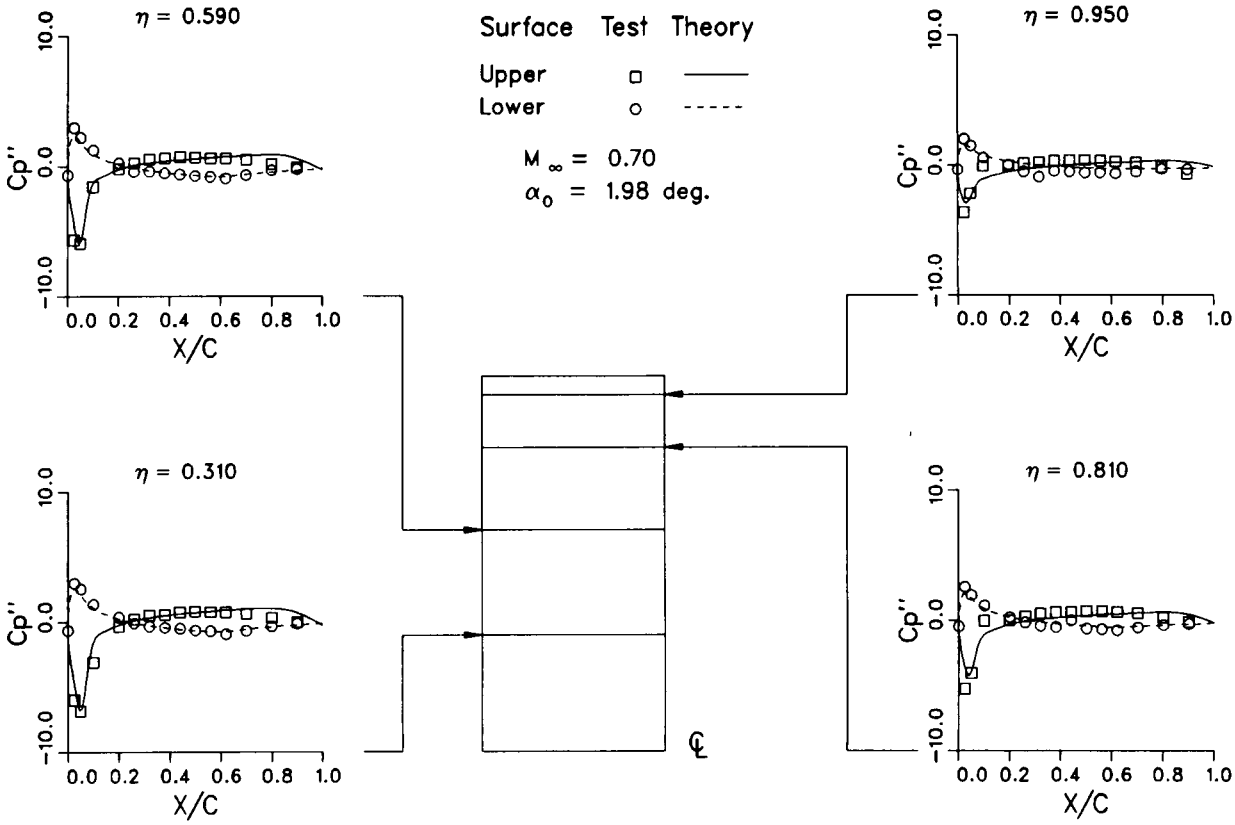

FIGURE 14. R376E21 INVISCID IMAGINARY AMPL=1.044 2000 S/C 5000 S (Concluded)

CONCLUDING REMARKS

A promising approach for the numerical solution of three-dimensional Euler and Navier-Stokes equations has been described. Additional work is needed for improving the efficiency of the present procedure. It is hoped that the techniques presented here will find use in fixed and rotary wing aircraft analysis. For additional studies and code correlations the reader is referred to Refs. 5-8.

1. A solution technique for the 3-D Euler and Navier-Stokes equations has been developed.

2. A number of interesting fixed and rotary wing applications have been presented.

3. Additional work towards improving the solution efficiency is now underway.

Figure 15

REFERENCES

1. Baldwin, B.S. and Lomax, H., "Thin Layer Approximation and Algebraic Model for Separated Turbulent Flows," AIAA Paper 78-0257.

2. Beam, R.F. and Warming, R.M., "An Implicit Finite-Difference Algorithm for Hyperbolic System in Conservation Law Form," Journal of Computational Physics, Vol. 22, p. 87, 1975.

3. Tung, C., Caradonna, F.X., Boxwell, D.A. and Johnson, W.R., "The Prediction of Transonic Flows on Advancing Rotors," Proceedings of the American Helicopter Society Annual Forum, May 1984.

4. Caradonna, F.X. and Tung, C., "Experimental and Analytical Studies of a Model Rotor in Hover," NASA TM 81232.

5. Sankar, L.N., Wake, B.E. and Lekoudis, S.G., "Solution of the Euler Equations for Fixed and Rotary Wing Configurations," Journal of Aircraft, Vol. 23, NO. 4, pp. 283-289, 1986.

6. Sankar, L.N., Malone, J.B. and Schuster, D., "Euler Solutions for Transonic Flow past a Fighter Wing," Journal of Aircraft, Vol. 24, No. 1, pp. 10-16, 1987.

7. Sankar, L.N. and Tung, C., "Euler Calculations for Rotor Configurations in Unsteady Forward Flight," Proceedings of the American Helicopter Society Annual Forum, June 1986.

8. Wake, B.E., "Solution Procedure for the Navier-Stokes Equations applied to Rotors," Ph.D. Dissertation, Georgia Institute of Technology, April 1987.